

**OPEN ACCESS**

# Assessment of Core-Shell and Agglomerate Particle Design for All-Solid-State Batteries

To cite this article: Walter Cistjakov *et al* 2022 *J. Electrochem. Soc.* **169** 050510

View the [article online](#) for updates and enhancements.



*Benefit from connecting  
with your community*

## ECS Membership = Connection

**ECS membership connects you to the electrochemical community:**

- Facilitate your research and discovery through ECS meetings which convene scientists from around the world;
- Access professional support through your lifetime career;
- Open up mentorship opportunities across the stages of your career;
- Build relationships that nurture partnership, teamwork—and success!

**Join ECS!**      **Visit [electrochem.org/join](https://electrochem.org/join)**





# Assessment of Core-Shell and Agglomerate Particle Design for All-Solid-State Batteries

Walter Cistjakov,<sup>1,2</sup> Vincent Laue,<sup>1</sup> Fridolin Röder,<sup>3</sup> and Ulrike Krewer<sup>2,4,z</sup> 

<sup>1</sup>Institute of Energy and Process Systems Engineering, TU Braunschweig, 38106 Braunschweig, Germany

<sup>2</sup>Cluster of Excellence SE<sup>2</sup>A Sustainable and Energy Efficient Aviation, Technische Universität Braunschweig, Germany

<sup>3</sup>Bavarian Center for Battery Technology (BayBatt), University of Bayreuth, 95447 Bayreuth, Germany

<sup>4</sup>Institute for Applied Materials—Electrochemical Technologies, Karlsruhe Institute of Technology, 76131 Karlsruhe, Germany

All-solid state lithium polymer batteries are promising next-generation batteries with high safety and energy density. Their success depends on an improved design with a tailored cathode manufacturing process. To facilitate a knowledge-driven optimal design of cathode, a model-based analysis on the impact of the cathode particle structure on the electrochemical cell performance is conducted. During production of solid-state cathodes, small active material particles such as lithium-iron phosphate tend to form large agglomerates with inner electrolyte-filled pores which have significant effect on transport properties within a secondary particle. Therefore, a battery cell model with secondary particles and optionally with a core-shell structure is developed and evaluated. Discharge performance is shown to be stronger impacted by changing the electrolyte fraction inside the particle than by changing the size of the electrolyte core within the secondary particle. A core-shell structure has a positive impact on the discharge performance and should be preferred for high power application. In contrast, cells with homogeneous agglomerate particles show better performance at low discharge rates. Thus, they are recommended for high energy and low power applications. The results of this study highlight the potentials of tailored production process for next-generation batteries.

© 2022 The Author(s). Published on behalf of The Electrochemical Society by IOP Publishing Limited. This is an open access article distributed under the terms of the Creative Commons Attribution 4.0 License (CC BY, <http://creativecommons.org/licenses/by/4.0/>), which permits unrestricted reuse of the work in any medium, provided the original work is properly cited. [DOI: 10.1149/1945-7111/ac67f8]



Manuscript submitted January 2, 2022; revised manuscript received April 5, 2022. Published May 5, 2022.

## List of symbols

$a_s$	specific surface area, $\text{m}^{-1}$
$c_e$	$\text{Li}^+$ concentration in electrolyte phase, $\text{mol m}^{-3}$
$c_s$	Li concentration in solid phase, $\text{mol m}^{-3}$
$C_{DL}$	double layer capacitance at the working electrode, $\text{C m}^{-2}$
$D_e$	salt diffusion coefficient in electrolyte, $\text{m}^2 \text{s}^{-1}$
$D_s$	lithium solid diffusion coefficient in solid phase, $\text{m}^2 \text{s}^{-1}$
$F$	Faraday constant, $\text{C mol}^{-1}$
$j^{\text{Li}}$	reaction current density, $\text{A m}^{-3}$
$j^{\text{tot}}$	total current density, $\text{A m}^{-3}$
$j^{\text{DL}}$	double layer current density, $\text{A m}^{-3}$
$k$	reaction rate constant, $\text{m}^4 \text{mol}^{-1} \text{s}^{-1}$
$R$	universal gas constant, $\text{J mol}^{-1} \text{K}^{-1}$
$R$	particle radius, $\text{m}$
$t$	time, $\text{s}$
$t_p$	transference number, —
$\alpha$	transfer coefficient, —
$\beta$	Bruggeman's exponent, —
$\delta$	thickness, $\text{m}$
$\varepsilon_s$	active material volume fraction, —
$\varepsilon_e$	electrolyte volume fraction, —
$\eta$	reaction overpotential, $\text{V}$
$\Phi_e$	electrical potential in electrolyte, $\text{V}$
$\Phi_s$	electrical potential in solid, $\text{V}$
$\sigma_e$	electrolyte conductivity, $\text{S m}^{-1}$
$\sigma_s$	electric conductivity, $\text{S m}^{-1}$

## Superscripts and subscripts

a	anode
agg	agglomerate phase
c	cathode
DL	double layer
e	electrolyte phase
max	maximum value
prim	primary particle

## (Continued).

OCP	open circuit potential
s	solid phase
sec	secondary phase
sep	separator
tot	total
0	initial value

All-solid state lithium batteries (ASSB) are considered to be promising candidates for safe battery systems with high energy density. By eliminating liquid components of the battery, disadvantages such as leakage and flammability of the electrolyte are avoided. Furthermore, an energy increase can be realized due to usage of pure lithium metal anodes. Nevertheless, several key challenges like low ionic conductivity and scalable processing for mass production are needed to have a breakthrough for this technology.<sup>1,2</sup>

A typical ASSB consists of a lithium metal anode and a composite cathode, including active material, solid electrolyte, conductive additive and binder. Both electrodes are separated by a separator. The structure and morphology of the cathode is crucial for battery high performance and high energy density.<sup>3</sup>

Laue et al. have proposed a model-based approach of a microstructure model of composite cathodes. It has shown that the structure, composition and distribution of cathode components have a strong influence on the effective electric and ionic conductivity.<sup>4</sup> Bielefeld et al. have also used a microstructure modeling approach and investigated the percolation of solid electrolyte and active material of a cathode to find the ideal composition for ASSB.<sup>5</sup> Strauss et al. compared large and small cathode active material particles in lithium-ion batteries (LIB) and ASSBs with a solid thiophosphate electrolyte. They have shown that active material particle size is crucial for the high performance of an ASSBs in contrast to LIBs. Discharge behavior of LIBs with different particle sizes was similar whereas ASSBs with small active material particles generated the highest discharge capacity.<sup>6</sup> Furthermore, Helmers et al. have investigated production processes which resulted in different cathode particle structures.<sup>7</sup> They proposed two scalable processes for solid polymer batteries based

<sup>z</sup>E-mail: [ulrike.krewer@kit.edu](mailto:ulrike.krewer@kit.edu)

on composite cathode granules with lithium iron phosphate (LFP) as active material. The granules consist of a solid polymer core and an active material and conductive additive shell. The first production process includes an additional extrusion step which leads to a homogeneously distributed polymer electrolyte. Whereas the second route leads to more inhomogeneous distribution and a lower rate capability. Cathode structure is thus an important one factor for improving the rate capability.<sup>7</sup> This kind of production can easily lead to agglomeration of LFP particles which is typically reported in literature.<sup>8</sup> Furthermore, the initial production step may cause a core-shell particle structure that either remains mostly unchanged without additional production steps, or it is further altered to large agglomerates in further production steps.

Core-shell particles have been reported in literature for batteries. Su et al. showed an overview about possible core-shell particle concepts.<sup>9</sup> All proposed concepts are mostly induced to balance different disadvantages of each component in a particle for improvement of battery performance. Sun et al. investigated experimentally core-shell particles consisting of two different active materials for cathode material. Here, the active material within the core has a high capacity and the shell a high thermal stability which combines the advantages of both materials.<sup>10</sup> Cho et al. reported a similar concept but with a different material combination.<sup>11</sup> All proposed experimental investigations have focused on LIB and none of them have considered core-shell particles with an electrolyte core for ASSB.

Modeling is recognized and used more and more to investigate batteries to reduce the high amount of trial-and-error experiments. Thus it leads the path toward knowledge-driven battery operation. Different modeling methods have been applied to investigate structural influences in batteries. These include classic pseudo-2-dimensional (P2D) models according to Doyle and Newman.<sup>12</sup> Such models have the advantage of moderate computational cost. Liu et al. employed a model-based approach to investigate mechanical influence during charge and discharge of core-shell particles consisting of a graphite core and a silicon shell.<sup>13</sup> Herein, they coupled mechanics and electrochemistry to investigate mechanical behavior of a battery cell. Further, Wu et al. used a model for core-shell particles to investigate the mechanical effect of lithiation and delithiation of two cathode active materials.<sup>14</sup> Their model has shown that independent mechanical stress within the shell and core during discharge and charge induce fracture and debonding of both particle areas. Lueth et al. proposed a P2D model with agglomerate active material particles.<sup>15</sup> They have investigated different properties of intrinsic and geometric parameters for agglomerate particles of  $\text{Li}(\text{Ni}_{0.33}\text{Co}_{0.33}\text{Mn}_{0.33})\text{O}_2$  active material. Nevertheless, they all

have focused on LIB which fast lithium transport properties of solid electrolytes and active material. A few models have recently been used for the investigation of polymer-based,<sup>16</sup> single-ion conducting<sup>17</sup> or thin film ASSBs,<sup>18</sup> but none of them focused on particle structures within the electrodes. 3D electrochemical models show a considerably higher computational cost. These models can take into account irregularities in the cell structure, though often limited to small cell sections.<sup>19</sup> Furthermore, there are 3D microstructure models of ASSBs that calculate effective parameters without performing electrochemical simulations.<sup>4,5</sup> They enable to determine, e.g. electric conductivity, ionic diffusivity and active surface area for arbitrary particle and pore size distributions as well as heterogeneous mixtures of active material, electrolyte and additives. Further, identified dependencies of effective parameters on composition of the electrode can be used to setup surrogate models. These microstructure models can be coupled with P2D models as shown by Laue et al., to more realistically evaluate batteries with different structures.<sup>20</sup>

All model-based and experimental works on core-shell particles have focused on either mixtures of two active materials or on single active materials but with agglomerate structure for liquid electrolyte batteries on a system level. Although, experimental work emphasizes the importance of the particle structure, currently no model-based approach exists of agglomerates or core-shell particles for ASSB. In this regard, we have focused our investigation on discharge behavior for cells with different secondary particle structures which consist of slow diffusive active materials and polymer based electrolytes to identify their limitations. This leads to the objective of this work which is to investigate discharge behavior of a polymer solid-state lithium battery cell and to give a recommendation for optimal cathode particle structure. For this purpose, a battery model with optionally agglomerate and core-shell particles is formulated. To the best knowledge of the authors, this is the first model to study core-shell structures in all solid-state batteries. The investigated battery cell consists of lithium iron phosphate (LFP) and a lithium metal foil as active materials for the cathode and anode, respectively. A polystyrene-*b*-polyethylene oxide (PS/PEO) with LiTFSI as conducting salt is used as polymer electrolyte in the separator as well as in the composite cathode.

## Mathematical Modeling

In the first part of this section, the geometrical structure of the model is described, followed by the electrochemical system and its equations, four investigated particle cases and the parameter set.

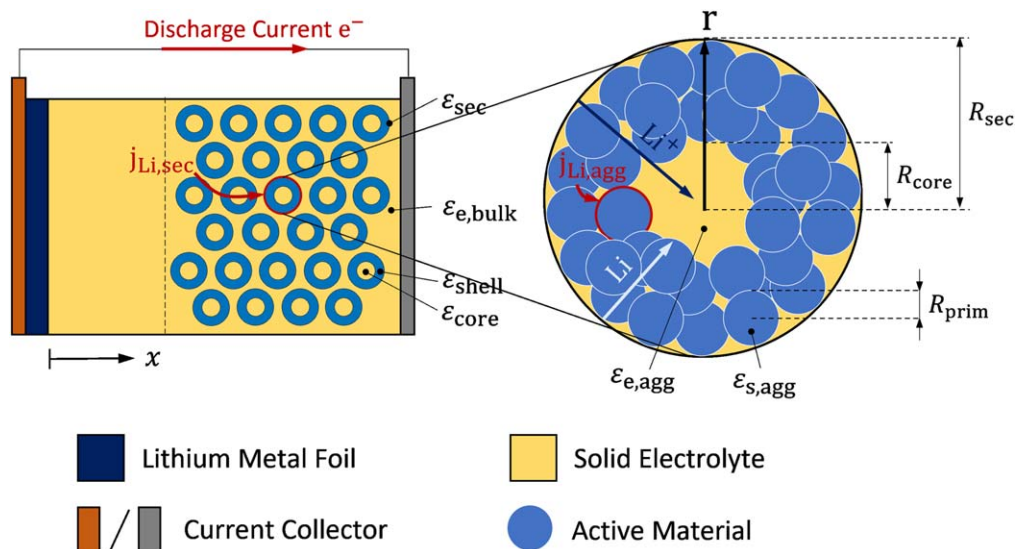


Figure 1. Overview of model containing porous LFP particles and electrolyte core.

**Electrode and core-shell particle geometries.**—The battery cell consists of a lithium anode and a composite cathode separated by a full solid polymer electrolyte separator. The cathode is completely filled with polymer electrolyte and active material without any voids in the overall structure. The polymer electrolyte serves as a binder, so that an additional additive is not necessary. The cathode structure is partitioned into a core-shell particle surrounded by electrolyte which is represented by particle fraction  $\epsilon_{\text{sec}}$  and outer electrolyte fraction within the electrode of electrolyte fraction  $\epsilon_{\text{e,bulk}}$  as can be seen in Fig. 1.

The cathode is modeled as a single spherical porous particles with radius  $R_{\text{sec}}$ , and consist of a core and a shell, based on a single particle model (SPM).<sup>21</sup> The SPM is applicable to cells with evenly distributed current densities along the electrode. The core is located in the center of the secondary particle. It has a radius  $R_{\text{core}}$  and consists entirely of electrolyte. The fraction of the core volume to secondary particle volume is defined as  $\epsilon_{\text{core}}$ . The shell encloses the core and thus occupies the remaining volume of the secondary particle. The shell takes up the volume fraction related to the secondary particle radius  $R_{\text{sec}}$  and its volume fraction can be described as follows:

$$\epsilon_{\text{shell}} = \frac{R_{\text{sec}}^3 - R_{\text{core}}^3}{R_{\text{sec}}^3} \quad [1]$$

where  $\epsilon_{\text{shell}}$  is the volume fraction of the shell inside the secondary particle. To determine the capacity of the entire cathode, the total volume of active material in the shells is required. It is assumed that the particle contains only electrolyte and active material. Thus the total volume fraction of the active material can be described as:

$$\epsilon_{\text{s,total}} = \epsilon_{\text{shell}} \cdot \epsilon_{\text{sec}} \cdot \epsilon_{\text{s,agg}} \quad [2]$$

with active material volume fraction within the shell  $\epsilon_{\text{s,agg}}$ .

The secondary particles are assumed to be spherical particles with radius  $R_{\text{sec}}$ , and they are as compact particles without any electrolyte, agglomerates, i.e. secondary particles with electrolyte in the pores, or as compact or agglomerated particles with a core-shell structure. In contrast to Lueth et al.,<sup>15</sup> the particles have a specific surface of the secondary particle depending on the particle radius. The outer surface area of the particle agglomerate is calculated as:

$$a_{\text{s,sec}} = \frac{3 \cdot \epsilon_{\text{sec}} \cdot \epsilon_{\text{s,agg}}}{R_{\text{sec}}} \quad [3]$$

$$a_{\text{s,agg}} = \frac{3 \cdot \epsilon_{\text{s,agg}}}{R_{\text{prim}}} \quad [4]$$

with  $R_{\text{prim}}$  being the radius of the primary particle. All equations in the particle are implemented in radial coordinates and all indexes in the particle are provided with agg.

The equations at cell level are in Cartesian coordinates in one-dimensional space and the indexes for this phase are provided with sec.

**Governing equations.**—In this section, the model of a solid state battery with polymer electrolyte and agglomerate or pore-shell type cathode particles is introduced. This electrochemical model is a modification of an agglomerate model by Lueth et al.<sup>15</sup> and a combination with an ASSB model with binary electrolyte based by Wu et al.<sup>16</sup> Hereby, the particles are implemented as superimposed phases of active material and electrolyte, similar as in the porous electrode theory.<sup>22</sup> Hereby agglomerate particles are considered to be secondary particle with radius,  $R_{\text{sec}}$ , that consist of optionally agglomerated LFP primary particles with a radius of  $R_{\text{prim}}$  as illustrated in Fig. 1.

LFP as active material is known as two-phase material with a Li-rich and Li-lean phase. Due to the two different phases, lithium diffusion in the solid phase of the active material changes during discharge, resulting in a diffusion coefficient change of  $10^{-18}$  to  $10^{-20} \text{ m}^2 \text{ s}^{-1}$ .<sup>23</sup> As this work focuses rather on secondary particles and electrode structure, where the principle interplay of design and processes is the focus, we use an average diffusion coefficient. However, we conducted simulations in the full range of the diffusion coefficients and were seeing negligible impact (see Appendix). All governing transport equations of the cell model, are summarized in Table I. Ion transport of  $\text{Li}^+$  and  $\text{TFSI}^-$  in the binary electrolyte is described using Nernst-Planck flux. Due to the monovalent ions ( $z_k; k \in \{\text{Li}^+, \text{TFSI}^-\}$ ) and assumption of electroneutrality ( $\sum_k z_k c_k = 0$ ) the transport equations for both species can be combined to the electrolyte transport (see Eq. 5). As a result, the influence of the charged species by migration can be represented only by the transference number  $(1 - t_p)$  in the term of the wall flux at the electrode surface.<sup>22,24</sup>

Thus, Eq. 5 consists of an accumulation term on the left side and a diffusion, production and flux term on the right side, where  $N_{\text{e,bulk}} = 0$  and  $j_{\text{Li,sec}} = 0$  in the separator phase. The additional flux term describes the local sink/source of electrolyte due to diffusion

**Table I. Equations for solid state battery model with core-shell particles.**

Model equations	Boundary Conditions
$\epsilon_{\text{e,bulk}} \frac{\partial c_{\text{e,bulk}}}{\partial t} = \frac{\partial}{\partial x} \left( D_{\text{e,bulk}}^{\text{eff}} \frac{\partial c_{\text{e,bulk}}}{\partial x} \right) + \frac{(1 - t_p) j_{\text{Li,sec}}}{F} + a_{\text{e,bulk}} N_{\text{e,bulk}} \quad [5]$	$\frac{\partial c_{\text{e,bulk}}(0)}{\partial x} = 0,$
$\epsilon_{\text{s,agg}} \frac{\partial c_{\text{s}}}{\partial t} = \frac{1}{r^2} \frac{\partial}{\partial r} \left( r^2 D_{\text{s}}^{\text{eff}} \frac{\partial c_{\text{s}}}{\partial r} \right) - \frac{j_{\text{Li,agg}}}{F} \quad [6]$	$\frac{\partial c_{\text{e,bulk}}(0)}{\partial x} = \frac{(1 - t_p) I}{A F}$
$\epsilon_{\text{e,agg}} \frac{\partial c_{\text{e,agg}}}{\partial t} = \frac{1}{r^2} \frac{\partial}{\partial r} \left( r^2 D_{\text{e}}^{\text{eff}} \frac{\partial c_{\text{e,agg}}}{\partial r} \right) + \frac{(1 - t_p) j_{\text{Li,agg}}}{F} \quad [7]$	$\frac{\partial c_{\text{s}}(0)}{\partial r} = 0, \quad \frac{\partial c_{\text{s}}(R_{\text{sec}})}{\partial r} = \frac{j_{\text{Li,sec}}}{a_{\text{s}} F}$
$j_{\text{tot}} = -\frac{\partial}{\partial x} \left( -\sigma_{\text{s}}^{\text{eff}} \frac{\partial \Phi_{\text{s}}}{\partial x} \right) \quad [8]$	$\frac{\partial c_{\text{e,agg}}(0)}{\partial r} = 0, \quad c_{\text{e,agg}}(R_{\text{sec}}) = c_{\text{e,bulk}}$
$j_{\text{tot}} = \frac{\partial}{\partial x} \left( -\sigma_{\text{e}}^{\text{eff}} \frac{\partial \Phi_{\text{e}}}{\partial x} \right) + \frac{\partial}{\partial x} \left( -\kappa_{\text{De}}^{\text{eff}} \frac{\partial \ln c_{\text{e,bulk}}}{\partial x} \right) \quad [9]$	$\frac{\partial \phi_{\text{s}}(0)}{\partial x} = \frac{I}{A \sigma_{\text{s,eff}}}, \quad \frac{\partial \phi_{\text{s}}(\delta_{\text{c}})}{\partial x} = 0$
	$\frac{\partial \phi_{\text{e}}(0)}{\partial x} = 0, \quad \phi_{\text{e}}(\delta_{\text{c}} + \delta_{\text{sep}}) = 0$

into or out of the secondary particle

$$N_{e,\text{bulk}} = D_{e,\text{agg}}^{\text{eff}} \frac{\partial c_{e,\text{agg}}(R_{\text{sec}})}{\partial r} \quad [10]$$

where  $D_{e,\text{agg}}^{\text{eff}}$  is the effective diffusion coefficient that takes porosity into account and  $c_{e,\text{agg}}$  the concentration of conductive salt in the electrolyte phase in the secondary particle.

The total current density  $j_{\text{tot}}$  for the simulated particle is composed of the double layer current  $j_{\text{DL}}$ , the reaction current at the secondary particle surface  $j_{\text{Li,sec}}$  and the reaction currents within the particle  $j_{\text{Li,agg}}$ . It is taken into account that the current density within the particle is calculated per corresponding radius. Hence, the total current density can be calculated by:

$$j_{\text{tot}} = j_{\text{DL}} + j_{\text{Li,sec}} + \frac{3}{R_{\text{par}}} \int_0^{R_{\text{par}}} r^2 j_{\text{Li,agg}} dr \quad [11]$$

Butler-Volmer equation is used to calculate the reaction current density at the secondary particle surface

$$j_{\text{Li,sec}} = a_{s,\text{sec}} i_{0,\text{sec}} \left( \exp\left(\frac{\alpha_a F \eta_{\text{sec}}}{RT}\right) - \exp\left(\frac{-\alpha_c F \eta_{\text{sec}}}{RT}\right) \right) \quad [12]$$

and the reaction current density within the particle at the primary particle surface area

$$j_{\text{Li,agg}} = a_{s,\text{agg}} i_{0,\text{agg}} \left( \exp\left(\frac{\alpha_a F \eta_{\text{agg}}}{RT}\right) - \exp\left(\frac{-\alpha_c F \eta_{\text{agg}}}{RT}\right) \right) \quad [13]$$

where  $a_{s,j}$  is the specific surface,  $i_{0,i}$  is the exchange current density and  $\eta_j$  is the overpotential of phase  $j$ . Further,  $\alpha_a$  and  $\alpha_c$  are the anodic and cathodic transfer coefficient, respectively,  $T$  is the operation temperature,  $F$  is the Faraday's constant and  $R$  is universal gas constant. The electrochemical double layer of the electrode is modeled by

$$j_{\text{DL}} = a_{s,\text{total}} C_{\text{DL}} \frac{\partial(\Phi_s - \Phi_e)}{\partial t} \quad [14]$$

where  $C_{\text{DL}}$  is the double layer capacitance,  $\Phi_s$  is the electric potential and  $\Phi_e$  is the ionic potential.  $a_{s,\text{total}}$  is the total specific surface area of the electrode composed of separate specific surfaces outside and within the secondary particle.

$$a_{s,\text{total}} = a_{s,\text{sec}} + a_{s,\text{agg}} \cdot \epsilon_{\text{sec}} \cdot \epsilon_{\text{shell}} \quad [15]$$

Here, the Li ions originating from the anode can either react at the outer surface ( $a_{s,\text{sec}}$ ), which corresponds to a non-porous secondary particle, or Li-ions diffuse into the electrolyte-filled secondary particle and react at the surface area of the primary particle ( $a_{s,\text{agg}} \cdot \epsilon_{\text{sec}} \cdot \epsilon_{\text{shell}}$ ). The exchange current density is determined according to the local concentrations at the surfaces. Thus, the exchange current density at the interface of the secondary particle can be calculated as follows

$$i_{0,\text{sec}} = k c_{e,\text{bulk}}^{\alpha_c} (c_{s,\text{max}} - c_s(R_{\text{sec}}))^{\alpha_a} c_s(R_{\text{sec}})^{\alpha_a} \quad [16]$$

where  $k$  is the reaction rate,  $c_s$  is the solid lithium concentration at the secondary particle radius,  $c_e$  the concentration in the electrolyte and  $c_{s,\text{max}}$  is the maximum concentration of the active material. The exchange current density within the particle can be described likewise by

$$i_{0,\text{agg}} = k c_{e,\text{agg}}(r)^{\alpha_c} (c_{s,\text{max}} - c_s(r))^{\alpha_a} c_s(r)^{\alpha_a} \quad [17]$$

Overpotential occurs at electrolyte-electrode interface of the secondary particle and primary particles and can be described as

$$\eta_{\text{sec}} = \Phi_s - \Phi_e - U_{\text{OCP}}(c_s(R_{\text{sec}})) \quad [18]$$

and

$$\eta_{\text{agg}} = \Phi_s - \Phi_e - U_{\text{OCP}}(c_s(r)) \quad [19]$$

where  $U_{\text{OCP}}(c_s)$  is the open circuit potential.

Effective transport parameters are calculated by the Bruggeman relation and a Bruggeman coefficient of  $\beta = 1.5$ .<sup>15</sup> Therefore, the following applies to the diffusion coefficient:

$$D_{j,i}^{\text{eff}} = D_{j,i} \cdot \epsilon_{j,i}^{\beta} \quad [20]$$

wherein  $D_{j,i}^{\text{eff}}$  is the effective,  $D_{j,i}$  is the free binary diffusion coefficient of species  $j \in \{\text{Li}, \text{Li}^+\}$  in phase  $i \in \{\text{active material, electrolyte}\}$  as well as  $\epsilon_{j,i}$  is the corresponding volume fraction.

The spatial discretization of the partial differential equations for the cell and the particle is done with a finite volume method and the time derivatives are solved with an ode solver embedded in Matlab. The boundary conditions for the model are listed in Table I on the right. Furthermore, all simulation parameters and initial values are taken from literature<sup>16,25,26</sup> and listed in Table II.

**Simulated particle structures.**—As already mentioned, particle structure could be a result based on the adjusted production process route.<sup>7</sup> Based on this idea four cases of particle structures are focused on: agglomerate, core-shell, compact and compact core-shell particles.

The core-shell particle as the base case scenario for all structures is represented by an electrolyte core radius ( $R_{\text{core}} > 0$ ) and an electrolyte fraction within the particle shell ( $\epsilon_{\text{agg}} > 0$ ) as illustrated in Fig. 2.

The case of evenly distributed active material primary particles within a secondary particle results in an agglomerate without any electrolyte core. Hence, the core radius is equal to zero ( $R_{\text{core}} = 0$ ) but an electrolyte fraction in-between primary particles still exists ( $\epsilon_{\text{agg}} > 0$ ). This means, mass transport within active material and electrolyte within secondary particle is possible as well as electrochemical reaction.

Secondary particles with electrolyte core ( $R_{\text{core}} > 0$ ) and no electrolyte structure within the shell of the secondary particle ( $\epsilon_{\text{agg}} = 0$ ) are called compact core shell particle. Due to the missing electrolyte phase in the shell, there is no ion mass transport within the shell. Last case is a compact particle which has no additional electrolyte structure within the secondary particle ( $R_{\text{core}} = 0$  &  $\epsilon_{\text{agg}} = 0$ ). That means that no ion transport is possible inside the particle so the electrochemical reaction only takes place at the outer surface of the secondary particle.

These structures allow to investigate the influence of electrolyte fraction within the particle on the discharge capacity and the influence of core size on the discharge behavior.

**Parameters.**—Modeling is conducted using Matlab 2019b. All used parameters in this simulation study are listed in Table II. Thickness of the cathode  $\delta_c$  is calculated for maximum usable thickness for a SPM. Details can be found in the Appendix. Thickness of the separator  $\delta_{\text{sep}}$  was chosen sufficiently small to make the transport effects within the particle predominant. Furthermore, for the electric conductivity  $\sigma_s$  was assumed that the conductivity additive is uniformly distributed in the solid phase of the secondary particle and thus in the electrode. A typical electrical conductivity used for LFP is  $0.5 \text{ S m}^{-1}$ , where no potential gradients are expected at the analyzed electrolyte fractions, thicknesses and C-rates.<sup>17</sup> Based on this, the analysis can focus on diffusion within the active material and electrolyte. The ionic conductivity  $\sigma_e$  is concentration dependent and is based on the work of Wu et al. to calculation the ionic resistance within the separator.<sup>16</sup> An Open-

**Table II. Base case parameter set for simulating the solid electrolyte battery cell.**

Parameter/Symbol	Value	Unit	References
Cathode thickness $\delta_c$	25	$\mu\text{m}$	—
Separator thickness $\delta_{\text{sep}}$	20	$\mu\text{m}$	—
Particle radius $R_{\text{sec}}$	2	$\mu\text{m}$	—
Particle radius $R_{\text{prim}}$	0.5	$\mu\text{m}$	—
Volume fraction particle $\varepsilon_{\text{s,total}}$	0.5	—	—
Volume fraction electrolyte on cell level $\varepsilon_{\text{e,bulk}}$	0.5	—	—
Max. Li concentration in the solid phase $c_{\text{s,max}}$	22806	$\frac{\text{mol}}{\text{m}^3}$	26
Electrolyte concentration $c_{\text{e},0}$	1200	$\frac{\text{mol}}{\text{m}^3}$	—
Anodic transfer coefficient $\alpha_a$	0.5	—	16
Cathodic transfer coefficient $\alpha_c$	0.5	—	16
Solid phase diffusion coefficient $D_s$	$8 \cdot 10^{-18}$	$\frac{\text{m}^2}{\text{s}}$	16
Electrolyte phase diffusion coefficient $D_e$	$7.8 \cdot 10^{-12}$	$\frac{\text{m}^2}{\text{s}}$	16
Electric conductivity $\sigma_s$	0.5	$\frac{\text{S}}{\text{m}}$	17
Ionic conductivity $\sigma_e$	$\sigma_e(c_e)$	$\frac{\text{S}}{\text{m}}$	16
Transference number $t_p$	0.41	—	16
Bruggeman's exponent $\beta$	1.5	—	25
Double layer capacitance $C_{\text{DL}}$	0.2	$\frac{\text{F}}{\text{m}^2}$	25
Reaction rate $k$	$5.03 \cdot 10^{-12}$	$\frac{\text{m}^4}{\text{mols}}$	16
Discharge rate $C_{\text{rate}}$	1	$\frac{1}{\text{h}}$	—

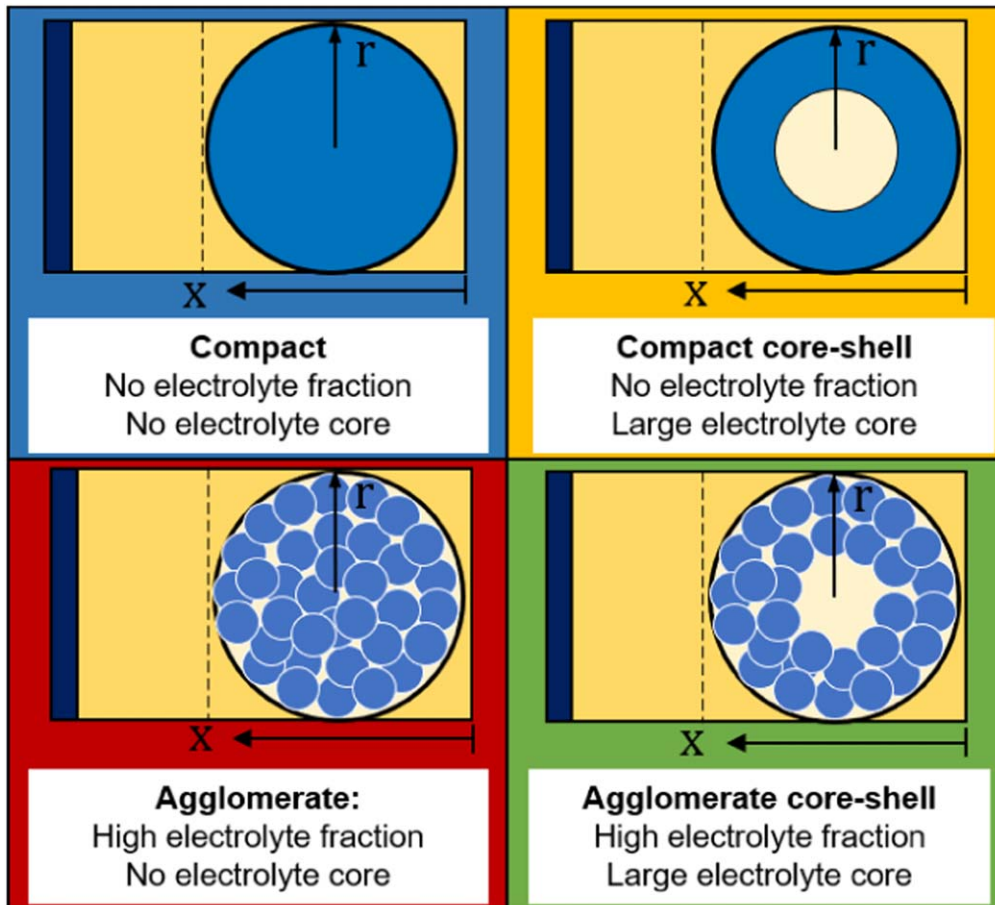


**Figure 2.** Variants of the ASSB model with different cathode particle structures.

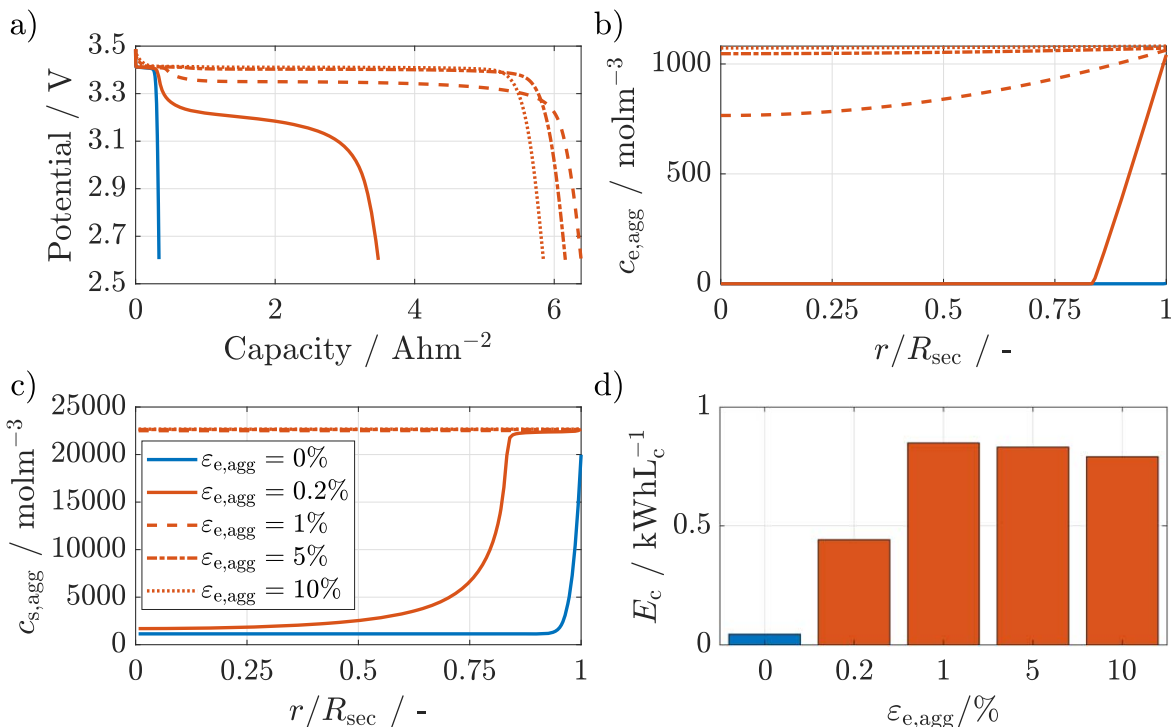


**Figure 3.** Analysis of the effect of electrolyte content of secondary particles on (a) discharge curves, (b) lithium ion concentration profiles in the electrolyte within the particle at the end of discharge, (c) lithium concentration in the active material within the secondary particle at the end of discharge (d) energy density per volume of active material within the cathode.  $C_{rate} = 1C$  and  $R_{sec} = 2 \mu m$ . Further parameters see Table II.

Circuit-Potential (OCP) curve is used for lithium-iron phosphate (LFP) from Ref. 26, which is a function of the state of charge (SOC) of the cathode active material. To understand the impact of electrode and particle geometry and thus to give a guideline for optimizing ASSB electrodes, the particle structures radius and electrolyte volume fraction are varied in this study and discharged at currents corresponding to a discharge rate of 1C. All other material-specific and geometric parameters are kept constant. These include electrolyte conductivity, electrolyte and active material diffusion coefficient and transference number according to Table II.

### Results and Discussion

In this section, first, cells containing compact particles are compared with cells containing agglomerate particles. This is followed by a comparison to cells with core-shell particles. Subsequently, C-rate tests reveal the influences of core-shell and agglomerate structures on the discharge behavior of the cells.

**Effect of using agglomerate particles.**—In Fig. 3, results for cells with agglomerate particles with various electrolyte fractions are shown. The electrolyte fraction correlates to the decrease in active material. Figure 3a shows the cell potential during the 1C-discharge process. The highest discharge capacity,  $6.3 \text{ Ah m}^{-2}$ , is observed for the electrolyte fraction of 1%. Compact particles, i.e. agglomerates with an electrolyte fraction of zero, show the lowest discharge capacity. Cells with electrolyte fractions larger than 5% exhibit decreasing capacity but higher potential throughout the discharge; this causes an intercept between the 1% and 5% discharge curves. For intermediate electrolyte fractions of 0.2 and 1%, two potential plateaus can be seen during discharge, where the first plateau ends at a similar capacity as the final capacity of the compact particle. To explain this behavior, we reveal the concentration profile of lithium within the active material and lithium ions within the electrolyte of the secondary particle at the end of discharge in Figs. 3b and 3c, respectively. It can be seen that the concentration in the electrolyte is decreasing with decreasing electrolyte fraction. This is caused by the

decreasing electrolyte volume fraction and consequently lower effective ionic transport and by consumption of lithium ions by reaction. That is why the lithium ion concentration is lowest in the center of the agglomerate particles, i.e.  $r \rightarrow 0$ . Further, it can be seen that for very low electrolyte fractions, here smaller 0.2%, lithium depletes within the electrolyte phase. As such, only a small part at the surface of the particle is active for the electrochemical reaction. This causes a low capacity and early voltage drop. In Fig. 3c, the corresponding lithium concentration within the active material is shown. It can be seen that the particles with high electrolyte fraction allow a full lithiation of the active material, which can be seen in constantly high lithium concentrations in the solid at the end of discharge. In contrast, lower electrolyte fractions yield low utilization of the active material in the center of the particle, i.e. toward normalized radius of zero. This is also in good agreement with the concentration in the electrolyte. It should be noted that two effects contribute to the observed profile and low capacity: the slow ion transport in the pores leads to a depletion of ions and thus of electrochemical reactions within the particle. In addition, diffusion of Li in the active material, LFP, is known to be very slow, so that produced Li accumulates only at the outer part of the particle. An even slower diffusion coefficient of  $1 \cdot 10^{-20} \text{ m}^2 \text{ s}^{-1}$ , which is representative for a Li-lean area of LFP active material, does not change the discharge behavior, nor the concentration profiles. For further details see Appendix.

This denotes that for LFP electrodes with low electrolyte fractions in agglomerated secondary particles the transport of lithium ions is limiting the battery discharge capacity. In addition, cells containing agglomerate particles with high electrolyte fractions above 1% also lead to low discharge capacities due to less active material. This explains why the discharge capacity is optimal for cells containing agglomerate particles with medium electrolyte fractions.

The total energy drawn from the battery is an integral of capacity and voltage. We therefore also analyze the effect of agglomerate porosity on energy density per cathode volume in Fig. 3d. Similar as for capacity, the lowest energy density is obtained by the cells with

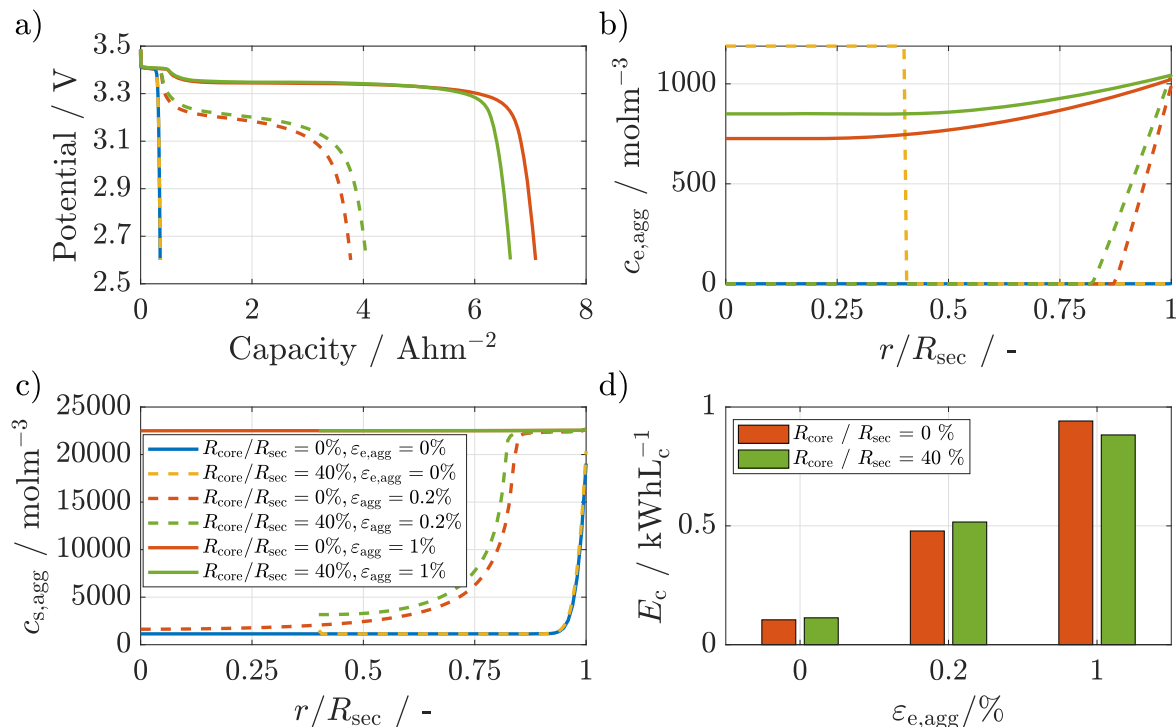


**Figure 4.** Analysis of the effect of electrolyte content and electrolyte core radius of secondary particles on (a) discharge curves, (b) lithium ion concentration profiles in the electrolyte within the particle at the end of discharge, (c) lithium concentration in the active material within the secondary particle at the end of discharge (d) energy density per volume of active material within the cathode.  $C_{rate} = 1C$  and  $R_{sec} = 2 \mu m$ . Further parameters see Table II.

electrolyte fraction of lower than 0.1%. Also similarly as for capacity, the energy density for 1% electrolyte fraction is the highest and is decreasing at higher electrolyte fractions for agglomerate particles. From this we can conclude that medium electrolyte fraction within agglomerate particles leads to higher utilization of active material, especially for slow lithium diffusion material such as LFP, as it shortens the solid diffusion paths by providing more active area and additional ionic conductive paths. With high electrolyte fraction, there is too few active material, so that the energy density decreases. Therefore, for agglomerate particles, there is the need to identify an optimal electrolyte fraction regarding energy and capacity. For our investigated LFP agglomerates particles of  $2 \mu m$ , 1% seems close to a local optimal electrolyte fraction.

**Effect of core-shell design.**—The previous analysis has shown that cells with an electrolyte fraction of 1% within a secondary particle exhibit a high capacity and almost full lithiation of active material particles at 1C discharge. Higher electrolyte fractions lead to better active material utilization but lower capacity. Therefore, 1% electrolyte fraction is chosen as upper limit for agglomerate core-shell particle investigation. In the following, the influence of an electrolyte core is investigated.

In Fig. 4, results for cells containing no vs electrolyte core spanning 40% of the particle radius in the secondary particle are compared. To elucidate the dependency on porosity of the particle shell, a non-porous shell is compared to a shell with a very low porosity of 0.2% and a shell with 1% porosity. Fig. 4a shows the potential evolution of the six cells during the discharge process. The highest capacity can be observed for agglomerate particles with 1% electrolyte fraction and no electrolyte core. On the other hand, cells with core-shell particles with 1% electrolyte fraction and an electrolyte core of 40% show a slightly higher cell potential through discharge while having a slightly lower capacity. Interestingly, the core-shell particle performs better for particles with a shell of 0.2% electrolyte content. Thus, core-shell particles may outperform particles without core. The lowest capacity can be observed for

cells having compact core-shell particles or compact particles without an electrolyte core.

For deeper insight, Figs. 4b and 4c show concentration profiles of lithium ions within the electrolyte and lithium within the active material of the secondary particle at the end of discharge, respectively. The lithium ion concentration within the electrolyte of a cell with core-shell particles and electrolyte fraction higher than  $\epsilon_{e,agg} > 0\%$  is always higher compared to cells with agglomerate particles. This is caused by the shorter diffusion paths of lithium ions in the electrolyte to the active surface area within the secondary particle for core-shell particles, both from outside and from the core, which constitutes an electrolyte reservoir. The lithiation takes place only in the shell ( $r/R_{sec} > 40\%$ ) thus in the core only lithium ion diffusion is possible. That is why the lithium-ion concentration within the electrolyte in the core ( $r/R_{sec} < 40\%$ ) is increasing from center to the inner boundary of the shell. In contrast, the cell with non-porous core-shell particles shows a constant lithium-ion concentration unaffected from beginning within the core because no connection to the counter electrode exists. This area is surrounded by the solid active material so that neither diffusion nor charge transfer reaction is possible.

The concentration for core-shell particles starts at the lower boundary of the shell ( $r/R_{sec} = 40\%$ ) because the active material is limited to the shell area of the secondary particle. It can be seen that cells with high electrolyte fraction of 1% in the particle accomplish full lithiation of active material, both for the cell without and with electrolyte core. This explains their high discharge capacity and voltage. In contrast, low electrolyte fraction results in a low utilization of active material in the center of the secondary particle for agglomerate and core shell particles. Furthermore, it can be seen that for cells with electrolyte fraction of 0.2% core-shell particles allow a higher lithium concentration compared to agglomerate particles. This can be explained by the shorter diffusion paths within the active material for core-shell particles because the diffusion is limited to the shell of the secondary particle. In addition, reserves of lithium ions in the electrolyte of the core support the charge transfer

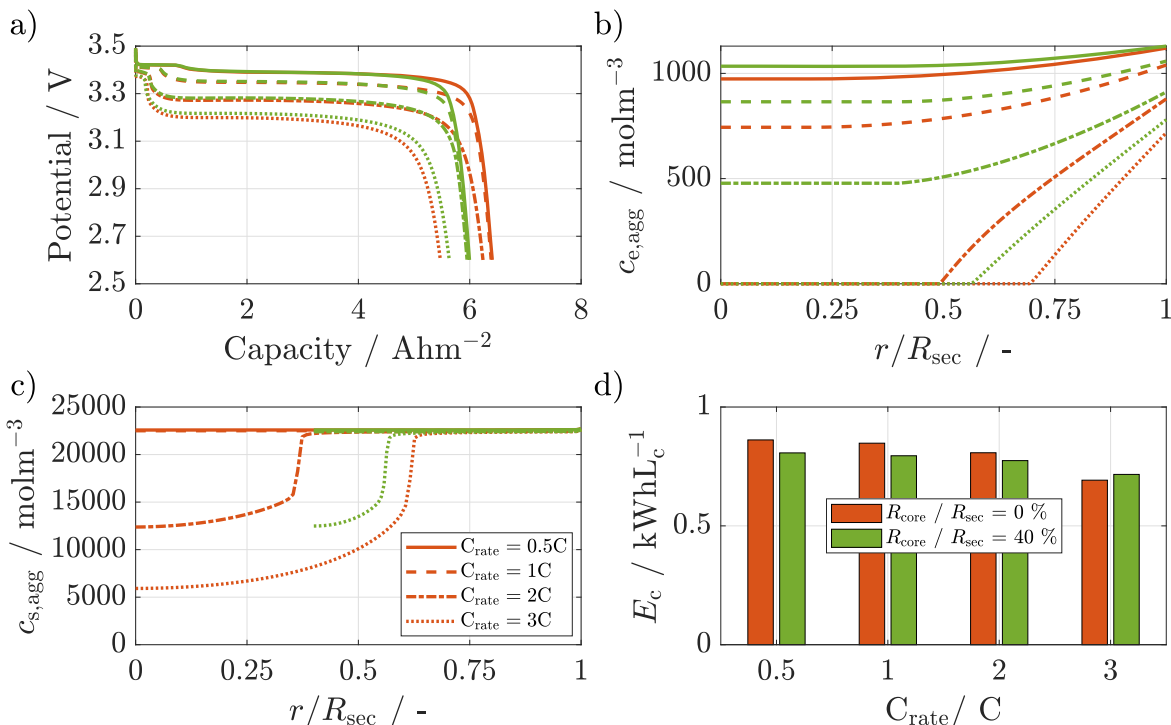


**Figure 5.** Analysis of the discharge rate on cells with and without an electrolyte core on (a) discharge curves, (b) lithium ion concentration in the electrolyte within the particle at the end of discharge, (c) lithium concentration in the active material within the secondary particle at the end of discharge (d) energy density per volume of active material within the cathode.  $R_{\text{core}}/R_{\text{sec}} = 0\%$  and  $40\%$ ,  $\varepsilon_{e,\text{agg}} = 1\%$  and  $R_{\text{sec}} = 2 \mu\text{m}$ . Further parameters see Table II.

reaction. LFP as active material has a slow solid diffusion which motivates short diffusion paths to achieve a high utilization. Further, in Fig. 4d the energy density per cathode volume is shown. It can be seen that cells with agglomerate particles and an electrolyte fraction of 1% have a higher energy density than cells with core-shell particles. This is in good agreement to the discharge capacity that can be explained by the higher amount of active material within the cathode. Cells with core-shell particles and 0.2% electrolyte fraction yield higher energy density compared to agglomerate particles due to their higher discharge capacity and voltage. As a result, cells with only agglomerate particles for low electrolyte fractions due to higher active material utilization for large LFP particles. For electrolyte fractions above 1% it changes and cells with agglomerate particles show the highest energy density, as they contain more active material. They thus pose the optimum between diffusion path lengths and fraction of active material.

**Effect of discharge rate vs particle design.**—The previous analysis revealed that agglomerate particles with 1% electrolyte fraction with and without core, both show a high and quite similar energy density during a 1C discharge. However, rate dependency is an important factor for real application. Therefore, we evaluate these cells also for three additional discharge rates.

Figure 5a shows that particles without core achieve at discharge rates of 0.5, 1 and 2C, higher capacities whereas the voltage plateau is the same. In contrast to this, at higher C-rates of 3C, cells with core-shell particles show higher capacity and voltage plateaus than those without core.

To understand the behavior, we exhibit the concentration profiles of lithium ions within the electrolyte and lithium within the active material of the secondary particle at the end of discharge in Figs. 5b and 5c, respectively. As expectable, the lithium-ion concentration within the electrolyte is decreasing with increasing discharge rate, i.e. consumption rate of Li in electrolyte. Furthermore, the quite low

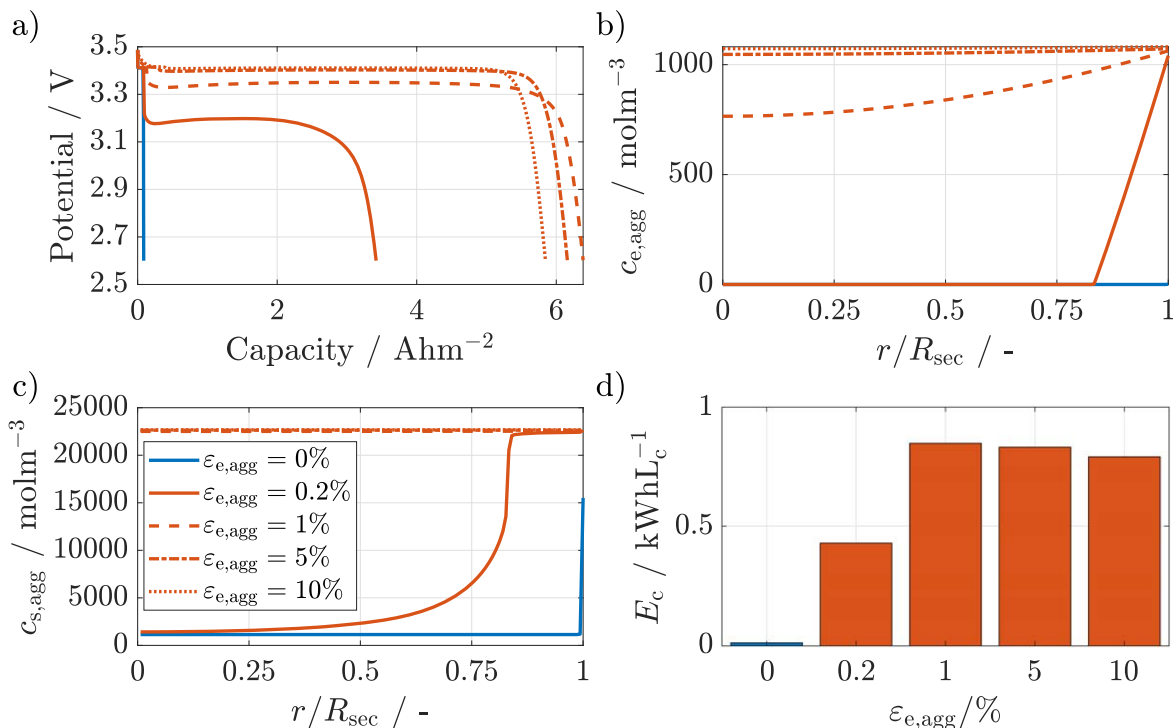
electrolyte fraction of 1% in the particle results in a slow diffusion of lithium ions into the secondary particle which leads to an electrolyte depletion within the center of the secondary particle at 2 and 3C discharge rate. Similar as discussed for 1C, for discharge rates below 2C the electrolyte concentration in core-shell particles is always higher than in agglomerate particles due to smaller diffusion distances and the additional electrolyte reservoir.

Figure 5c shows that for 0.5 and 1C discharge rate a complete lithiation in both particle structures is reached due to sufficiently fast diffusion. In contrast to this for fast discharge rates, the concentration is decreasing in particle center direction. Here, the diffusion through the active material and electrolyte are too slow and limit the discharge performance. Except for the cell with core-shell particles and a C-rate of 2C that is completely lithiated. Lithium and lithium ions are accumulating at the surface of the secondary particle and lead to high overpotentials and a fast voltage drop. Again, cells with core-shell particles have a higher lithiation compared to cells with agglomerate particles due to shorter diffusion paths.

Figure 5d shows that for low C-rates of 0.5, 1 and 2C cells with agglomerate particles achieve higher energy densities than with core-shell particles at 0.5, 1 and 2C. This is due to the sufficient time for diffusion and higher amount of active material within agglomerate particles. Cells with core-shell particles have a higher energy density at 3C compared to cells with agglomerate particles. This is due to higher capacity and higher voltage of cells with core-shell particles because they have shown a higher lithiation. To sum it up, cells with core-shell structures for agglomerate particles are preferable at high discharge rates. In this case, high energies can be realized despite slow transport kinetic in the active material and large secondary particles due to higher active material utilization. On the other hand, agglomerate particles show better performance at slow discharge due to more active mass. Charge simulations of analyzed cells were performed, but showed similar features compared to the discharge behavior, leading to rapid potential rises in cells with dense particles and high charge capacities in cells with

**Table III.** Variation of the cathode thickness and corresponding voltage drops at 1C and 3C discharge rate based on the initial ionic and electric conductivity of 0.0338 S/m and 0.5 S/m, respectively.

Cathode thickness $d_{\text{cat}}$ in $\mu\text{m}$	Voltage drop at 1 C in V	Voltage drop at 1 C in V
25	0.0099	0.0297
30	0.0143	0.0428
35	0.0194	0.0582
40	0.0253	0.0760
45	0.0321	0.0962
50	0.0396	0.1188

**Figure 6.** Analysis of the effect of electrolyte content of secondary particles on (a) discharge curves, (b) lithium ion concentration profiles in the electrolyte within the particle at the end of discharge, (c) lithium concentration in the active material within the secondary particle at the end of discharge (d) energy density per volume of active material within the cathode.  $C_{\text{rate}} = 1\text{C}$  and  $R_{\text{sec}} = 2\ \mu\text{m}$   $D_s = 1 \cdot 10^{-20}\ \text{m}^2\text{s}^{-1}$ . Further parameters see Table II.

high electrolyte fraction with the agglomerate particle. Therefore, the charge processes were not considered in more detail.

### Conclusions

This work contributes to understanding the effect of cathode particle structures in all solid-state polymer cells on discharge behavior and energy density. Focus was laid on small LFP particles that typically agglomerate. Depending on the electrode production process, agglomerated particles, solid particles or particles even with electrolyte in its core may be expected. To optimize electrode design, our modeling work therefore compared the performance of agglomerate core-shell particles, compact core-shell particles, agglomerate particles and compact particles. Cells with agglomerated, i.e. porous particles lead to better active material utilization and so to higher energy densities compared to cells with compact particles. Cells with electrolyte fraction of 1% performed best and reached the highest energy density.

Thereby, cells without an electrolyte core in the particles have shown higher capacity but lower active material utilization. Especially, core-shell particles with low electrolyte fraction can reach a full lithiation and perform better than cells with agglomerate particles because of shorter diffusion paths within the active

material. This is why core-shell particles are preferable when the electrolyte fraction within the secondary particle is very low. Nevertheless, it should be noted, that high electrolyte fraction within the secondary particle can lead to contact losses between primary particles, which means that active material is isolated and not usable. To prevent this, additional conductive additives can be added to increase the percolation paths and thus the electric conductivity. Additional 3D microstructure models, as in Laue et al.,<sup>4,20</sup> can be used to investigate and optimize percolation paths within a particle and resulting effective parameters, i.e. effective electric and ionic conductivity.

Finally, the influence of the discharge rate on secondary particles with and without electrolyte core and an electrolyte fraction of 1% was analyzed. For low discharge rates, cells without electrolyte core in the particles yielded the highest capacity and energy density. In contrast to this, cells with core-shell particles performed better at high discharge rates because of higher active material utilization. This is due to shorter diffusion paths in core-shell particles, which decreases the effect of slow solid lithium diffusion in LFP and leads to higher energy densities.

In this study we focused on cathode particle structure and its effect on the discharge performance. The results motivate practical studies toward identifying production routes that enable the

production of electrodes with the identified optimal particle structure, i.e. size, porosity and core-size. As not all structures may be producible to sufficient accuracies, we foresee a fruitful interaction of model-based identification of well performing particle structures and feasible structures produced in the practical production process. With our model, we could clearly show general trends in how and how far particle structure impacts performance of ASSBs. Future models may dig deeper into certain particle structures, the impact of particle surface modification, non-idealities at the Li metal<sup>27,28</sup> and by multiple solid phases.<sup>23</sup> The extensions will be relevant for quantitative prediction of experimental results and to understand non-idealities.

### Acknowledgments

This work was supported by the German Federal Ministry for Economic and Affairs of Energy through funding the project "FesKaBat—Feststoff-Kathoden für zukünftige Hochenergie-Batterien" (03ET6092D) and we would like to acknowledge the funding by the Deutsche Forschungsgemeinschaft (DFG, German Research Foundation) under Germany's Excellence Strategy—EXC 2163/1—Sustainable and Energy Efficient Aviation—Project-ID 390 881 007.

### Appendix

**Potential gradient.**—The assumption of a single particle model requires a uniform current density distribution along the cathode to be applicable. For this purpose, the voltage drop along the electrode is investigated that determines the distribution of the current density. This voltage drop can be calculated with the ionic and electric conductivity to calculate the voltage drop based on Ref. 29:

$$\Phi_{\text{drop}} = C_A \cdot C_{\text{rate}} \cdot R_{\text{tot}} \quad [\text{A} \cdot \text{I}]$$

Hereby,  $C_A$  is the areal capacity of the cell and  $R_{\text{tot}}$  the total resistance of the cathode based on the effective ionic and electric conductivity, calculated by the Bruggeman relation in Eq. 20. All results were checked for a 1C and 3C discharge rate and are listed in Table III. A criterion of maximum of 30 mV was used as a limit. It can be seen, that for a cathode thickness of 25  $\mu\text{m}$  a voltage drop lower than the maximum limit for a 3C discharge rate was reachable. Thicker cathodes do not fulfill the requirement and so the thickness for performed simulation was set to 25  $\mu\text{m}$ .

**Slow LFP diffusion coefficient.**—In Section 3.1, a constant diffusion coefficient of  $8 \cdot 10^{-18} \text{ m}^2 \text{ s}^{-1}$  for lithium transport within active material is used. LFP is a two-phase material, therefore we investigated a slow diffusion coefficient of  $1 \cdot 10^{-20} \text{ m}^2 \text{ s}^{-1}$  which corresponds to diffusion in the Li-lean phase to compare the effect on cell performance.<sup>23</sup> When comparing Figs. 3 and 6, we can see almost identical discharge curve, concentration profiles and energy densities. Small changes are visible only in the progression of the discharge curves, which show for the slow diffusion a slight minimum at low capacities.

### ORCID

Ulrike Krewer  <https://orcid.org/0000-0002-5984-5935>

### References

1. C. Sun, J. Liu, Y. Gong, D. P. Wilkinson, and J. Zhang, "Recent advances in all-solid-state rechargeable lithium batteries." *Nano Energy*, **33**, 363 (2017).
2. Q. Zhang, K. Liu, F. Ding, and X. Liu, "Recent advances in solid polymer electrolytes for lithium batteries." *Nano Research*, **10**, 4139 (2017).

3. J. Betz, G. Bieker, P. Meister, T. Placke, M. Winter, and R. Schmuch, "Theoretical versus Practical Energy: A Plea for More Transparency in the Energy Calculation of Different Rechargeable Battery Systems." *Adv. Energy Mater.*, **9**, 1803170 (2019).
4. V. Laue, N. Wolff, F. Röder, and U. Krewer, "Modeling the Influence of Mixing Strategies on Microstructural Properties of All-Solid-State Electrodes." *Energy Technology*, **8**, 1801049 (2020).
5. A. Bielefeld, D. A. Weber, and J. Janek, "Microstructural Modeling of Composite Cathodes for All-Solid-State Batteries." *The Journal of Physical Chemistry C*, **123**, 1626 (2019).
6. F. Strauss, T. Bartsch, L. de Biasi, A.-Y. Kim, J. Janek, P. Hartmann, and T. Brezesinski, "Impact of Cathode Material Particle Size on the Capacity of Bulk-Type All-Solid-State Batteries." *ACS Energy Lett.*, **3**, 992 (2018).
7. L. Helmers, L. Froböse, K. Friedrich, M. Steffens, D. Kern, P. Michalowski, and A. Kwade, "Sustainable Solvent-Free Production and Resulting Performance of Polymer Electrolyte-Based All-Solid-State Battery Electrodes." *Energy Technology*, **9**, 2000923 (2021).
8. Z. Yang, Y. Dai, S. Wang, and J. Yu, "How to make lithium iron phosphate better: a review exploring classical modification approaches in-depth and proposing future optimization methods." *Journal of Materials Chemistry A*, **4**, 18210 (2016).
9. L. Su, Y. Jing, and Z. Zhou, "Li ion battery materials with core-shell nanostructures." *Nanoscale*, **3**, 3967 (2011).
10. Y.-K. Sun, S.-T. Myung, M.-H. Kim, J. Prakash, and K. Amine, "Synthesis and Characterization of  $\text{Li}[(\text{Ni}_{0.8}\text{Co}_{0.1}\text{Mn}_{0.1})(\text{Ni}_{0.5}\text{Mn}_{0.5})_{0.2}]\text{O}_2$  with the Microscale Core-Shell Structure as the Positive Electrode Material for Lithium Batteries." *J. Am. Chem. Soc.*, **127**, 13411 (2005).
11. Y. Cho, S. Lee, Y. Lee, T. Hong, and J. Cho, "Spinel-Layered Core-Shell Cathode Materials for Li-Ion Batteries." *Adv. Energy Mater.*, **1**, 821 (2011).
12. M. Doyle, T. F. Fuller, and J. Newman, "Modeling of Galvanostatic Charge and Discharge of the Lithium/Polymer/Insertion Cell." *J. Electrochem. Soc.*, **140**, 1526 (1993).
13. B. Liu, X. Wang, H.-S. Chen, S. Chen, H. Yang, J. Xu, H. Jiang, and D.-N. Fang, "A Simultaneous Multiscale and Multiphysics Model and Numerical Implementation of a Core-Shell Model for Lithium-Ion Full-Cell Batteries." *Journal of Applied Mechanics*, **86** 041005 (2019).
14. B. Wu and W. Lu, "Mechanical Modeling of Particles with Active Core-Shell Structures for Lithium-Ion Battery Electrodes." *The Journal of Physical Chemistry C*, **121**, 19022 (2017).
15. S. Lueh, U. S. Sauter, and W. G. Bessler, "An Agglomerate Model of Lithium-Ion Battery Cathodes." *J. Electrochem. Soc.*, **163**, A210 (2016).
16. S.-L. Wu, A. E. Javier, D. Devaux, N. P. Balsara, and V. Srinivasan, "Discharge Characteristics of Lithium Battery Electrodes with a Semiconducting Polymer Studied by Continuum Modeling and Experiment." *J. Electrochem. Soc.*, **161**, A1836 (2014).
17. N. Wolff, F. Röder, and U. Krewer, "Model Based Assessment of Performance of Lithium-Ion Batteries Using Single Ion Conducting Electrolytes." *Electrochimica Acta*, **284**, 639 (2018).
18. D. Danilov, R. A. H. Niessen, and P. H. L. Notten, "Modeling All-Solid-State Li-Ion Batteries." *J. Electrochem. Soc.*, **158**, A215 (2011).
19. C.-W. Wang and A. M. Sastry, "Mesoscale Modeling of a Li-Ion Polymer Cell." *J. Electrochem. Soc.*, **154**, A1035 (2007).
20. V. Laue, F. Röder, and U. Krewer, "Joint structural and electrochemical modeling: Impact of porosity on lithium-ion battery performance." *Electrochimica Acta*, **314**, 20 (2019).
21. J. Li, R. G. Landers, and J. Park, "A comprehensive single-particle-degradation model for battery state-of-health prediction." *Journal of Power Sources*, **456**, 227950 (2020).
22. J. Newman and W. Tiedemann, "Porous-electrode theory with battery applications." *AIChE J.*, **21**, 25 (1975).
23. V. Srinivasan and J. Newman, "Discharge Model for the Lithium Iron-Phosphate Electrode." *J. Electrochem. Soc.*, **151**, A1517 (2004).
24. M. Doyle and J. Newman, "The use of mathematical modeling in the design of lithium/polymer battery systems." *Electrochimica Acta*, **40**, 2191 (1995).
25. N. Legrand, S. Raël, B. Knosp, M. Hinaje, P. Desprez, and F. Lapique, "Including double-layer capacitance in lithium-ion battery mathematical models." *Journal of Power Sources*, **251**, 370 (2014).
26. M. Farkhondeh, M. Safari, M. Pitzker, M. Fowler, T. Han, J. Wang, and C. Delacourt, "Full-Range Simulation of a Commercial  $\text{LiFePO}_4$  Electrode Accounting for Bulk and Surface Effects: A Comparative Analysis." *J. Electrochem. Soc.*, **161**, A201 (2014).
27. T. Liu, J. Zheng, H. Hu, O. Sheng, Z. Ju, G. Lu, Y. Liu, J. Nai, Y. Wang, W. Zhang, and X. Tao, "In-situ construction of a Mg-modified interface to guide uniform lithium deposition for stable all-solid-state batteries." *Journal of Energy Chemistry*, **55**, 272 (2021).
28. O. Sheng et al., "In Situ Construction of a LiF-Enriched Interface for Stable All-Solid-State Batteries and its Origin Revealed by Cryo-TEM." *Adv. Mater.*, **32**, 2000223 (2020).
29. S. Randau et al., "Benchmarking the performance of all-solid-state lithium batteries." *Nat. Energy*, **5**, 259 (2020).